ASIAN JOURNAL OF CIVIL ENGINEERING (BHRC) VOL. 17, NO. 1 (2016)
PAGES 43-57

MODIFIED EXPLICIT SCHEME OF RETURN MAPPING INTEGRATION ALGORITHM ON ROTATIONAL HARDENING CONSTITUTIVE MODEL FOR CLAY

A. Shirmohammadi, M. Hajialilue Bonab* and S. Soleymani Shishvan
University of Tabriz, Faculty of Civil Engineering, Tabriz, Iran.

Received: 21April 2015; **Accepted:** 10 August 2015

ABSTRACT

Natural clay soils due to anisotropy have a different behavior from disturbed and remolded specimens. The Modified Cam Clay (MCC) model, as a fundamental critical state model, cannot capture this behavior with enough accuracy. However, anisotropic models that known as rotational hardening models can efficiently simulate the anisotropic behavior. Specifically, SANICLAY model, which has been recently developed, has a high accuracy in modeling of the anisotropy and thus is used in the present study. Here, a semi-explicit constitutive integration scheme is proposed and validated for the SANICLAY model. It is then implemented in FLAC software through a UDM subroutine. Several triaxial simmulations are carried out and the results are compared with the MCC model results. Advantages of the proposed integration method in terms of stability, accuracy and speed are discussed.

Keywords: constitutive integration; semi-explicit scheme; SANICLAY; rotational hardening

1. INTRODUCTION

Soils in general, exhibit some degree of anisotropic behavior which may be quite considerable depending on their formation, composition, structure and prior loading history. Many natural soil deposits have a transverse isotropic structure in which the material properties are equal in all directions in the horizontal plane but are different from vertical direction which is the direction of the soil deposition. This type of anisotropy is also called cross anisotropy. Casagrande and Carillo [1] were the first who categorize anisotropy of soils into inherent and induced types. Inherent anisotropy is essentially related to the physical composition prior to any loading that is established during the natural deposition

*E-mail address of the corresponding author: mhbonab@gmail.com (M. Hajialilue-Bonab)

and consolidation process. This anisotropy is generally obtained from the micro-structure (soil fabric, inter-particle bonding, and arrangement) of the soils, but may also be due to the macro-structure (fissures, joints, laminations, etc.). Induced anisotropy is a result of loading history and inelastic deformation in the post depositional stage. Whittle [2] discusses that "real" soils often contain some induced anisotropy as part of their stress history which makes the distinction between the inherent and induced anisotropy to be difficult. Another definition of anisotropy is given by Ladd et al. [3] in types of initial and evolving. Initial anisotropy is a combination of inherent anisotropy and anisotropic initial shear strength but the evolving anisotropy is same as the induced anisotropy defined by Casagrande and Carillo [1].

Extensive research conducted by several investigators (e.g., [4-5]) has emphasized a need for considering the anisotropy of soils in the design and analyses of geotechnical structures. Over the past four decades, an increasing awareness of the importance of anisotropy of cohesive soils has led to considerable research including laboratory, field, theoretical and numerical studies. The improvement and development of professional testing devices and experimental techniques have also contributed to continuous and extensive research on soil anisotropy. Numerous experimental studies have been so far focused on the strength and stiffness anisotropy. These studies have been covered a wide range of tests including triaxial and biaxial compression and extension tests, simple, direct, and torsional shear tests on soil samples in drained and undrained conditions. Wide laboratory studies on the anisotropic behavior of Boston Blue Clay (BBC) have been done over the years by MIT researchers, e.g. [6]. Similar anisotropic tests on other types of clay have been carried out by other investigators [7-8]. According to these laboratory studies the degree of initial anisotropy significantly influences the pore water pressure and stress–strain–strength response of an anisotropically consolidated clay specimen under undrained shearing. All these experiments provide extensive evidence of the significance of initial anisotropy on the strength and deformation behavior of the soils. Experimental observations also indicate that for K_0-consolidated clays the yield surface is oriented along a line close to the K_0 line (e.g. [3] and [9]).

In the numerical analyses of geotechnical problems, in which the soil has a significant degree of anisotropy, neglecting soil anisotropy may lead to an oversimplification and unrealistic soil response. Therefore, various constitutive models that consider soil anisotropy have been proposed over the past three decades. There are several approaches to simulate the soil anisotropy. One class of anisotropic plasticity model is based on the concept of multi-surfaces that are associated with a kinematic hardening rule to incorporate induced anisotropy [10-11]. Another approach is based on a multi-laminate framework [12-13] in which the induced anisotropy and the effect of rotation of principal stress axes are intrinsically taken into account without requiring additional material parameters. Inherent anisotropy can be included by introducing a structural variant.

Rotational and in some cases distortional and mixed isotropic hardening laws have also been shown to be suitable candidates for modeling anisotropic behavior. By introducing a rotational hardening tensor in a general multiaxial formulation (or a scalar-valued rotational hardening variable in triaxial formulation), the rotation and/or distortion of the yield surface and plastic potential due to initial and induced anisotropy can be described. Many of the existing anisotropic models for cohesive soils are based on the framework of critical state soil mechanics [14-18].

The simplest energetic extension of the Modified Cam clay (MCC) model [19] from isotropic to anisotropic behavior has been proposed by Dafalias [16]. Based on the rotational hardening law and plastic potential proposed by Dafalias [16] several anisotropic models have been introduced and developed [20-21]. The so called SANICLAY model [22] that refers to as "Simple ANIsotropic CLAY" is also an extension of the model proposed in [16] with a nonassociated flow rule. To consider an inherent anisotropy, Taiebat et al. [23] incorporated the destructuration theory within the SANICLAY framework.

In the present work, SANICLAY is used to study the effect of anisotropy on the response of geotechnical structures founded on cohesive soils. The model is selected because of its simplicity and its capability to provide reasonably accurate response of clayey soils. The identification and determination of the model parameters may be the most critical factor affecting the selection of the model to be empliyed in practical problems. Most sophisticated models have a large number of parameters, some of which cannot be readily obtained from laboratory tests. SANICLAY model requires only three additional parameters over those needed by the MCC model that can calibrate with previous experimental test data.

In Section 2, a brief description of the SANICLAY model is provided. Then, the proposed semi-explicit integration algorithm is presented in Section 3. Its implementation within FLAC software is also addressed in Section 4. Finally, Section 5 presents the numerical results obtained for several cases.

2. DESCRIPTION OF THE CONSTITUTIVE MODEL

SANICLAY is a nonassociated elastoplastic model that is constructed within the framework of critical state soil mechanics. Dafalias et al. [16] have described the model in a triaxial formulation where a step-by-step generalization of the model to a triaxial space has been given. Here, a brief description of the model in triaxial space is recapitulated.

Formulation of the model is presented in the triaxial stress–strain space in terms of stress quantities $p = (\sigma_a + 2\sigma_r)/3$ and $q = (\sigma_a - \sigma_r)$ as well as strain quantities $\varepsilon_v = (\varepsilon_a + 2\varepsilon_r)$ and $\varepsilon_q = 2(\varepsilon_a - \varepsilon_r)/3$ where subscripts a and r denote the axial and the radial directions of a triaxial sample, respectively. The stress ratio is denoted by $\eta = q/p$.

2.1 Elastic response

The conventional hypoelastic stress–strain relations in the rate form are given as:

$$\dot{\varepsilon}_v^e = \frac{\dot{p}}{K}, \quad \dot{\varepsilon}_q^e = \frac{\dot{q}}{3G} \tag{1}$$

where K and G are elastic bulk and shear moduli, respectively. The elastic bulk modulus can be obtained by $K = p(1 + e_{in})/\kappa$, where e_{in} is the initial value of void ratio and κ is the slope of swelling line in the e-ln(p) space.

It is noted that natural cohesive soils may also exhibit anisotropy in their elastic response, i.e. cross-anisotropy after deposition and consolidation [24]. While elastically anisotropic behavior can be incorporated in the constitutive relation, it brings in more complexities to the model formulation with additional material parameters that may not be easily obtained.

Moreover, SANICLAY has been developed particularly to be used with normally consolidated or lightly over-consolidated cohesive soils where a modest increase in stress may cause yielding, and thus plastic deformations are likely to dominate for the problems of interest.

2.2 Plastic potential and yield function

In a triaxial stress space, the shape of plastic potential, shown in Fig. 1, is a rotated and distorted ellipse which can be described as [21].

$$g = (q - p\alpha)^2 - (M^2 - \alpha^2)p(p_\alpha - p) = 0 \tag{2}$$

where α is a rotational hardening parameter that controls both the rotation and distortion of the plastic potential. Here, p_α is the value of p at $q = p\alpha$ and should be set to satisfy the pair of p and q values at yield in Equation (2) and M is the critical state line slope in q-p space. Clearly, one must have $|\alpha| < M$ for real valued p and q in Equation (2). Note that $M = M_c$ when the stress ratio $\eta = q/p > \alpha$ and $M = M_e$ when the stress ratio $\eta = q/p \leq \alpha$ [21].

The yield function postulates same form as that of the plastic potential function with rotational hardening parameter β, which is given as [21]:

$$f = (q - p\beta)^2 - (N^2 - \beta^2)p(p_0 - p) = 0 \tag{3}$$

where p_0 represents isotropic hardening parameter that is defined as the value of p at $\eta = \beta$ and controls the size of the yield surface. Clearly, one must have $|\beta| < N$ for real valued p and q in Equation (3).

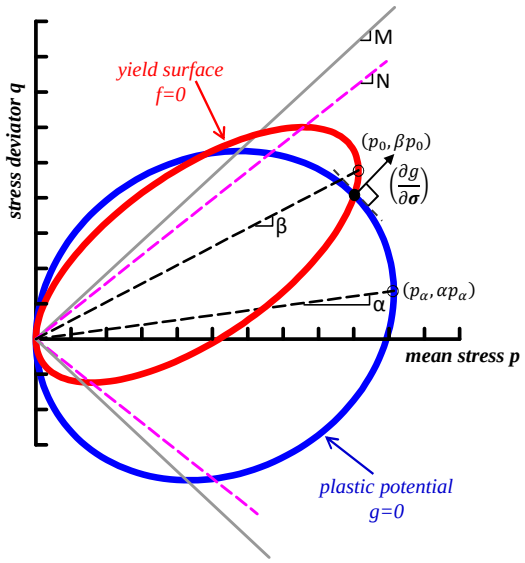

Figure 1. Yield surface and plastic potential surface in triaxial stress space.

2.3 Flow rule

The corresponding equations for the volumetric and deviatoric plastic strain rates are given by a nonassociated flow rule as

$$\dot{\varepsilon}_v^p = \langle \dot{L} \rangle \frac{\partial g}{\partial p}, \quad \dot{\varepsilon}_q^p = \langle \dot{L} \rangle \frac{\partial g}{\partial q} \tag{4}$$

where $\dot{L}$ is the loading index (or plastic multiplier). "$\langle\ \rangle$" denotes Macauley brackets, i.e. $\langle \dot{L} \rangle = \begin{cases} \dot{L} \ for \ \dot{L} > 0 \\ 0 \ \ for \ \dot{L} \leq 0 \end{cases}$. Substitution of equation (2) into (4) gives rise to

$$\dot{\varepsilon}_v^p = \langle \dot{L} \rangle \frac{\partial g}{\partial p} = \langle \dot{L} \rangle p(M^2 - \eta^2), \quad \dot{\varepsilon}_q^p = \langle \dot{L} \rangle \frac{\partial g}{\partial q} = \langle \dot{L} \rangle 2p(\eta - \alpha) \tag{5}$$

2.4 Hardening laws

Here, evolution laws for the hardening parameters of the model, i.e. p_0, α and β are presented. It is noted that p_α serves only to adjust the size of g = 0; so that g goes through any point (p, q) on f = 0. The isotropic hardening which describes the classical evolution law of the yield surface is given by [21].

$$\dot{p}_0 = \langle \dot{L} \rangle \bar{p}_0 = \langle \dot{L} \rangle \left(\frac{1 + e_{in}}{\lambda - \kappa} \right) p_0 \left(\frac{\partial g}{\partial p} \right) \tag{6}$$

where λ is the slope of the normal compression line in the e-ln(p) space. The evolution of rotational hardening parameter of plastic potential α, which represents the degree of anisotropy, is defined by [21].

$$\dot{\alpha} = \langle \dot{L} \rangle \bar{\alpha} = \langle \dot{L} \rangle \left(\frac{1 + e_{in}}{\lambda - \kappa} \right) C \left(\frac{p}{p_0} \right)^2 \left| \frac{\partial g}{\partial p} \right| |\eta - x\alpha| (\alpha^b - \alpha) \tag{7}$$

where C and x are model constants that control the rate of evolution of anisotropy and saturation limit of anisotropy, respectively, and α^b is *α-bounding* that specifies the authorized boundary of rotational hardening of potential surface. Note that, if $\eta/x > \alpha$, α^b must equal to M_c and if $\eta/x < \alpha$, α^b must equal to M_e.

The evolution of rotational hardening parameter of yield surface β is given as [21].

$$\dot{\beta} = \langle \dot{L} \rangle \bar{\beta} = \langle \dot{L} \rangle \left(\frac{1 + e_{in}}{\lambda - \kappa} \right) C \left(\frac{p}{p_0} \right)^2 \left| \frac{\partial g}{\partial p} \right| |\eta - \beta| (\beta^b - \beta) \tag{8}$$

where β^b is *β-bounding* that specifies the authorized boundary of rotational hardening of yield surface. Note that, if $\eta > \beta$, β^b must equal to N and if $\eta < \beta$, β^b must equal to $-N$.

2.5 Plastic multiplier and plastic modulus

The plastic multiplier $\dot{L}$ and plastic modulus K_p are obtained by standard methods of

plasticity by applying the consistency condition $\dot{f} = 0$ which states that the stress state must always lie on the yield surface. By appling $\dot{f} = 0$ to Equation (3) and in conjunction with Equations (6) and (8) we have

$$K_p = -\left(\frac{\partial f}{\partial p_0}\bar{p}_0 + \frac{\partial f}{\partial \beta}\bar{\beta}\right) = p\left[(N^2 - \beta^2)\bar{p}_0 + 2(q - p_0\beta)\bar{\beta}\right] \tag{9}$$

$$\dot{L} = \frac{1}{K_p}\left(\frac{\partial f}{\partial p}\dot{p} + \frac{\partial f}{\partial q}\dot{q}\right) = \frac{1}{K_p}p[(N^2 - \eta^2)\dot{p} + 2(\eta - \beta)\dot{q}] \tag{10}$$

where $\bar{p}_0$ and $\bar{\beta}$ are given in equations (6) and (8), respectively.

3. SEMI-EXPLICIT INTEGRATION SCHEME

To use the constitutive models in a nonlinear analysis of boundary value problems, the rate equations described in the previous section need to be numerically integrated over a time increment. The integration scheme and the corresponding algorithm control the accuracy, convergence, and stability characteristics of the solution. The integration schemes can be extensively classified into implicit and explicit, for which many different types are proposed. Both implicit and explicit integration schemes have been so far used to integrate constitutive models for soils and other materials.

A comprehensive experssion on various implicit integration schemes for elastoplastic models can be found in [25], among others. Implicit integration schemes have successfully been used in integration of various constitutive models for soils [26-29]. It has been shown that with implicit integration schemes a quadratic convergence and unconditional stability for Newton–Raphson iterations can be achieved with the use of a material (consistant) Jacobian. Stability and quadratic convergence are guaranteed for classical plasticity models such as J_2-plasticity. However, this may not be true for more complex models with high nonlinearities. The second derivatives of the yield and plastic potential functions are needed in the algorithm as well as for the construction of material Jacobian. It is often a lengthy and cumbersome procedure to obtain the closed-form derivatives for complex models, if they can be derived at all, and their implementation is not always straightforward.

On the other hand, for the explicit integration schemes, higher-order derivatives of the yield and plastic potential functions are not needed and the implementation of the algorithms is generally straightforward. While their simplicity and general applicability seem to be attractive features, a major drawback of explicit integration schemes is that the algorithm is conditionally stable which means that an appropriate step size must be used to retain numerical stability.

Here, we propose a so called semi-explicit integration scheme which is constructed based on the return mapping method [30]. It will be shown that the proposed method is quite simple as well as efficient when applied for the constitutive laws in SANICLAY model. The essential features of the integration scheme are highlighted and details of the integration algorithm are provided in the following sub-sections.

3.1 Integration algorithm

In the semi-explicit integration scheme of return mapping method, the first step involves an elastic predictor in which a trial stress is calculated by assuming an elastic response, is given

$$\sigma_{ij}^{\text{trial}} = \sigma_{ij}^{\text{old}} + C_{ijkl}^{e}\,\Delta\varepsilon_{kl} \tag{11}$$

where σ_{ij}^{old} is the previos step stress, C_{ijkl}^{e} is the linear elastic material multiplier (Hooke's law) and $\Delta\varepsilon_{kl}$ is a strain increment. Deviator stresses can be define as

$$s_{ij}^{\text{trial}} = \sigma_{ij}^{\text{trial}} - \frac{1}{3}\sigma_{ij}^{\text{trial}}\,\delta_{ij} \tag{12}$$

where δ_{ij} is a Kronecker delta. Stress invariants define as

$$p^{\text{trial}} = -\frac{1}{3}\sigma_{ii}^{\text{trial}}, \quad q^{\text{trial}} = \sqrt{\frac{3}{2}s_{ij}^{\text{trial}}\,s_{ij}^{\text{trial}}} \tag{13}$$

This trial stress state may lie inside the yield surface, in which case, the response is elastic and the trial stress is the new stress state. However, if the trial stress lies outside the yield surface, the stress state must be corrected and brought back onto the yield surface in order to satisfy the consistency condition. Note that the yield surface in essence evolves due to the hardening. The flow rule defines the plastic strain rate. However, within a numerical scheme, this has to be handled with some appropriate assumptions so that the plastic strain increment can be determined. Here, we propose to use

$$\Delta\varepsilon^{p} = \Delta L\,(\frac{\partial g}{\partial \sigma})^{\text{trial}} \tag{14}$$

so that, new stresses in the triaxial stress space are given as

$$p^{\text{new}} = p^{\text{trial}} - K\Delta\varepsilon_{v}^{p} = p^{\text{trial}} - K\Delta L\left(\frac{\partial g}{\partial p}\right)^{\text{trial}} \tag{15}$$

$$q^{\text{new}} = q^{\text{trial}} - 3G\Delta\varepsilon_{q}^{p} = q^{\text{trial}} - 3G\Delta L\left(\frac{\partial g}{\partial q}\right)^{\text{trial}} \tag{16}$$

where the return mapping concept is adopted. These stresses must satisfy the yield function according to the consistency condition. Substituting equations (15) and (16) into equation (3) leads to a quadratic equation to be solved with respect to ΔL as

$$a\Delta L^{2} + b\Delta L + c = 0 \tag{17}$$

with

$$a = 9G^2\left(\left(\frac{\partial g}{\partial q}\right)^{\text{trial}}\right)^2 - 6\beta GK\left(\frac{\partial g}{\partial p}\right)^{\text{trial}}\left(\frac{\partial g}{\partial q}\right)^{\text{trial}} + N^2K^2\left(\left(\frac{\partial g}{\partial p}\right)^{\text{trial}}\right)^2 \tag{18}$$

$$\begin{aligned} b = -6Gq^{\text{trial}}\left(\frac{\partial g}{\partial q}\right)^{\text{trial}} + 2\beta q^{\text{trial}}K\left(\frac{\partial g}{\partial p}\right)^{\text{trial}} + 6\beta pG\left(\frac{\partial g}{\partial q}\right)^{\text{trial}} + N^2p_0K\left(\frac{\partial g}{\partial p}\right)^{\text{trial}} \\ - \beta^2p_0K\left(\frac{\partial g}{\partial p}\right)^{\text{trial}} - 2N^2p^{\text{trial}}K\left(\frac{\partial g}{\partial p}\right)^{\text{trial}} \end{aligned} \tag{19}$$

$$c = (q^{\text{trial}} - p^{\text{trial}}\beta)^2 - (N^2 - \beta^2)p^{\text{trial}}\left(p_0 - p^{\text{trial}}\right) \tag{20}$$

Here,

$$\left(\frac{\partial g}{\partial p}\right) := p(M^2 - \eta^2), \quad \left(\frac{\partial g}{\partial q}\right) := 2p(\eta - \alpha) \tag{21}$$

and it is assumed that the hardening parameters do not evolve during the updating process of stress state. Given the value of ΔL, p^{new} and q^{new} are calculated through equations (15) and (16) and thus stresses are obtained by

$$\sigma_{ij}^{\text{new}} = s_{ij}^{\text{new}} + p^{\text{new}}\delta_{ij} \tag{22}$$

where

$$s_{ij}^{\text{new}} = s_{ij}^{\text{trial}}\frac{q^{\text{new}}}{q^{\text{trial}}} \tag{23}$$

Similarly, the plastic volumetric strain is given as

$$\Delta\varepsilon_v^p = \Delta L\left(\frac{\partial g}{\partial p}\right)^{\text{trial}} \tag{24}$$

Specific volume can also be calculated as

$$v^{\text{new}} = v_0(1 + \Delta\varepsilon_v) \tag{25}$$

where $\Delta\varepsilon_v = \Delta\varepsilon_{ii}$ and $v_0 = 1 + e_{in}$ is the initial value of specific volume. Bulk modulus is then updated through

$$K^{\text{new}} = \frac{v^{\text{new}}p^{\text{new}}}{\kappa} \tag{26}$$

Isotropic hardening parameter is similarly updated as

$$p_0{}^{\text{new}} = p_0{}^{\text{old}} + \Delta L\left(\frac{v^{\text{new}}}{\lambda-\kappa}\right) p_0{}^{\text{old}} \left(\frac{\partial g}{\partial p}\right)^{\text{trial}} \tag{27}$$

and rotational hardening parameter of potential surface is updated as

$$\alpha^{\text{new}} = \alpha^{\text{old}} + \Delta L\left(\frac{v^{\text{New}}}{\lambda-\kappa}\right) C\left(\frac{p^{\text{New}}}{p_0}\right)^2 \left|\left(\frac{\partial g}{\partial p}\right)^{\text{trial}}\right| \left|\eta^{\text{New}} - x\alpha^{\text{old}}\right|\left(\alpha^b - \alpha^{\text{old}}\right) \tag{28}$$

Finally, for the rotational hardening parameter of yield suface, we have

$$\beta^{\text{new}} = \beta^{\text{old}} + \Delta L\left(\frac{v^{\text{new}}}{\lambda-\kappa}\right) C\left(\frac{p^{\text{new}}}{p_0}\right)^2 \left|\left(\frac{\partial g}{\partial p}\right)^{\text{trial}}\right| \left|\eta^{\text{new}} - \beta^{\text{old}}\right|\left(\beta^b - \beta^{\text{old}}\right) \tag{29}$$

The way adopted to update the hardening parameters makes the integration scheme explicit.

4. NUMERICAL IMPLEMENTATION

The above mentioned constitutive integration of SANICLAY model is implemented in the commercial finite difference software (2D) FLAC with the User-Defined Constitutive Models UDM provided in FLAC. Although an extended version of the MCC model is available in FLAC, for proper comparison of the two models, the MCC model is also implemented with UDM using a similar semi-explicit integration algorithm. The details of the implementation of MCC model follow that of the SANICLAY model with a few changes according to the constitutive laws. The implemented MCC model is validated against in-built MCC model within the FLAC for several drained and undrained triaxial compression tests with various OCRs.

5. SIMULATION RESULTS AND DISCUSSIONS

SANICLAY requires a calibration of eight constant model parameters (see Table 1). The first five parameters are same as those in the MCC model and are easily calibrated using the data obtained from standard laboratory tests. The calibration of the last three parameters (*N*, *x* and *C*) can also be done by adopting the procedure proposed in [21]. SANICLAY model is calibrated for LCT based on the experimental data presented by Gens [7]. The calibrated values of the eight parameters for SANICLAY are represented in Table 1.

5.1 Undrained shearing

First, the data of undrained triaxial compression (CK_0UC) and extension tests (CK_0UE) on K_0-consolidated specimens of LCT with OCR = 1, 2, 4 and 7 are considered. Simulations are carried out using the SANICLAY and MCC models and the results are presented within *q- p* space which are normalized by σ_{max}^{axial} as the maximum axial (vertical) stress of the preceding consolidation path. Moreover, results are presented by plotting variations of q vs ε_{axial}.

Table 1: Calibrated parameters for LCT [21]

Parameter	Description of role	Value
M_c	Value of stress ratio at critical state in compression	1.18
M_e	Value of stress ratio at critical state in extension	0.86
λ	Compressibility of normally consolidated clay	0.063
κ	Compressibility of over-consolidated clay	0.009
ν	Elastic Poisson's ratio	0.2
N	Shape of the yield surface	0.91
x	Saturation limit of anisotropy (under path with constant stress ratio)	1.56
C	Rate of evolution of anisotropy	16

The stress–strain response and the stress paths obtained using the SANICLAY model for several values of OCRs are shown in Fig. 2. As discussed in [21], the model simulations are comparable to the experimental data by Gens [7]. It is illustrated that the SANICLAY model shows reasonable agreement for normally consolidated specimens (OCR=1) with the experiments.

To emphasize the significant capabilities brought in by the anisotropic model, the same experiments are simulated by using the MCC model. The simulation results are shown in Fig. 3. The severe limitation of the predictive capability of the MCC model in modeling the response of an anisotropic soil is clear from these results in which shear strength is overestimated for triaxial extension tests. Moreover, the MCC model lacks the essential ingredients to account for softening during undrained shear loading (after the initial anisotropic consolidation) which many cohesive soils exhibit.

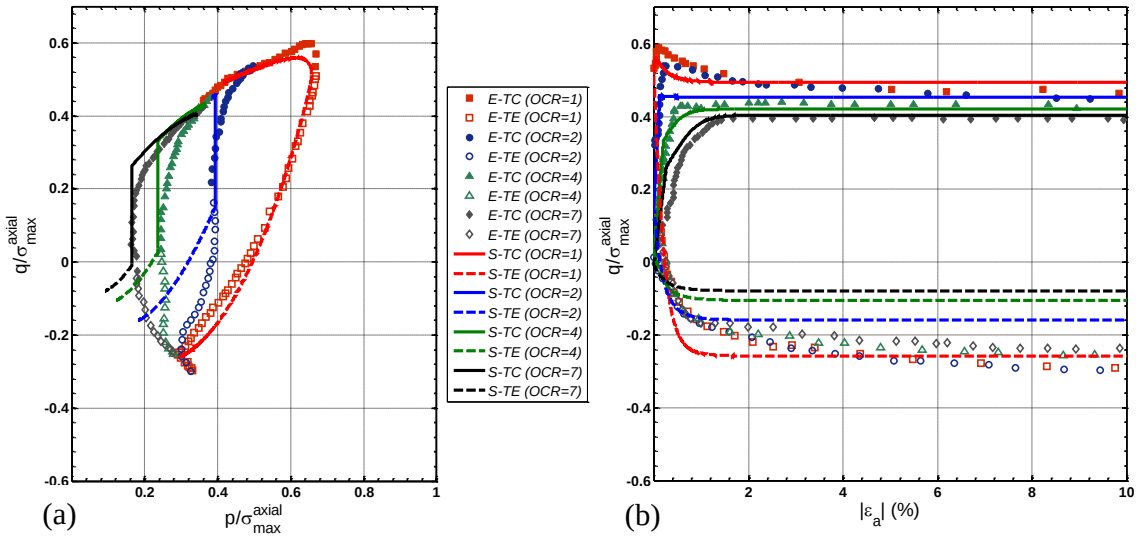

Figure 2. Comparison of SANICLAY simulations with experimental data for undrained triaxial tests on K_0-consolidated samples of LCT with various OCR values (Gens [7]). **E-TC** and **E-TE** are abbreviations for experimental compression and extension tests, respectively; while **S-TC** and **S-TE** are for simulation results of the compression and extension tests, respectively

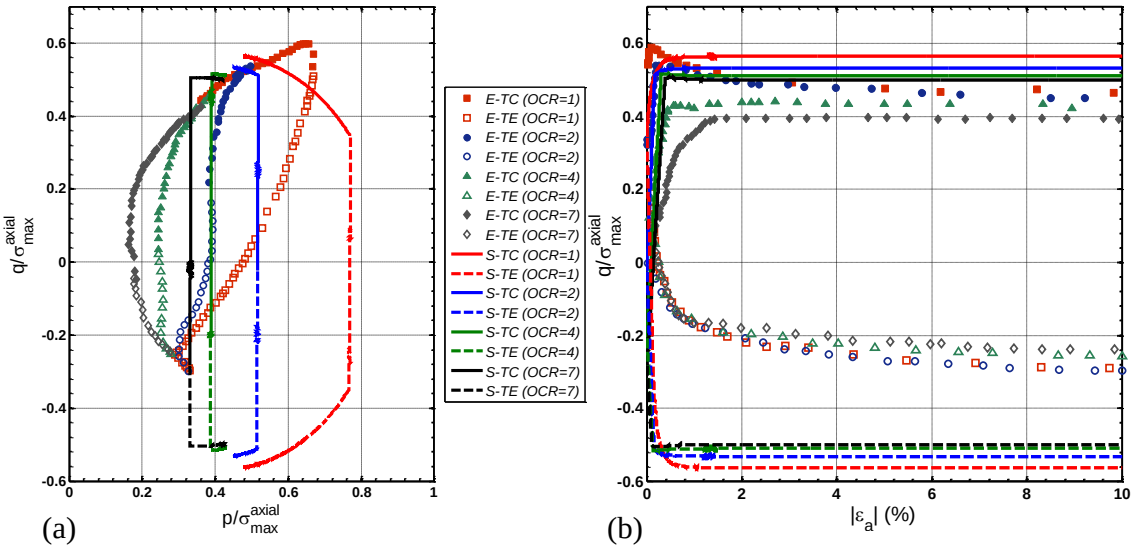

Figure 3. Comparison of MCC simulations with experimental data for undrained triaxial tests on K_0-consolidated samples of LCT with various OCR values (Gens [7]). See caption of Fig. 2 for definitions of abbreviations

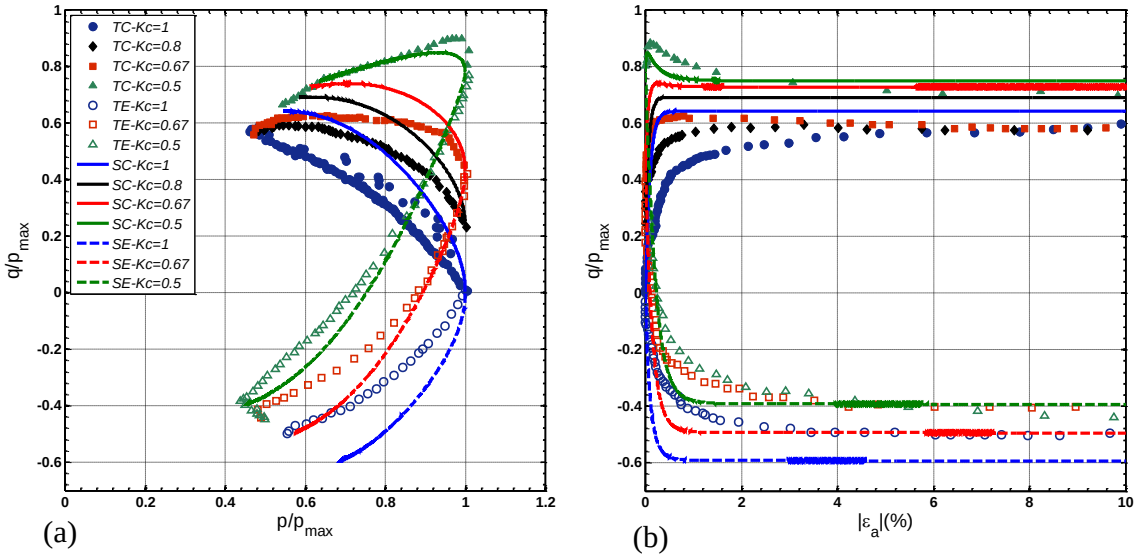

Figure 4. Comparison of SANICLAY simulations with experimental data for undrained triaxial tests on anisotropically consolidated samples of LCT and OCR = 1, (Gens [7]). **TC-K_c** and **TE-K_c** are abbreviations for the experimental compression and extension tests, respectively; while **SC-K_c** and **SE-K_c** are for the simulation of compression and extension tests, respectively

The effects of consolidation history and therefore induced anisotropy on the undrained shearing response are unavoidable. Especially, the differences are larger for OCR = 1 compared to OC samples. Therefore, for better portraying these effects, Fig. 4 compares the data and the simulations for undrained triaxial compression (CAUC) and extension tests

(CAUE) on anisotropically consolidated samples of LCT with OCR = 1. The comparison of simulation and experimental test is made in the q- p space normalized by p_{max}, i.e. the maximum mean effective stress of the preceding consolidation path. The various tests are differentiated in terms of the value of the consolidation stress ratio $K_c = \sigma_{r,c}/\sigma_{a,c}$, i.e. the ratio of the radial effective stress over its axial effective stress during consolidation. For example, the TC and TE tests with $K_c = 0.5$ correspond to the CK_0UC and CK_0UE tests for OCR = 1 of Fig. 2. As expected, the best agreement between the simulations and experiments is obtained for $K_c = 0.5$, because these two tests were used for the calibration of SANICLAY as discussed in [21]. Generally, the performance of the model improves as the K_c approaches the value 0.5.

5.2 Drained shearing

To complete the validation/verification of the proposed integration scheme, the drained triaxial compression (CK_0DC) tests on K_0-consolidated specimens of LCT with OCR = 1, 1.5, 2, 4 and 7 are illustrated in Fig.5. In particular, Fig.5 (a) makes the comparison in terms of the shear stress–strain response, while Fig.5 (b) does the same in terms of the volumetric strain ε_v. It is seen that the shear stress–strain response is better simulated than the volumetric strain for all values of OCR. More specifically, the model simulates successfully the $q/\sigma_{max}^{axial} - \varepsilon_{axial}$ response, with the an exception of the softening response for OCR = 7. Moreover, the volumetric ε_v strain is successfully simulated, specially for high OCRs (i.e. OCR = 4–7).

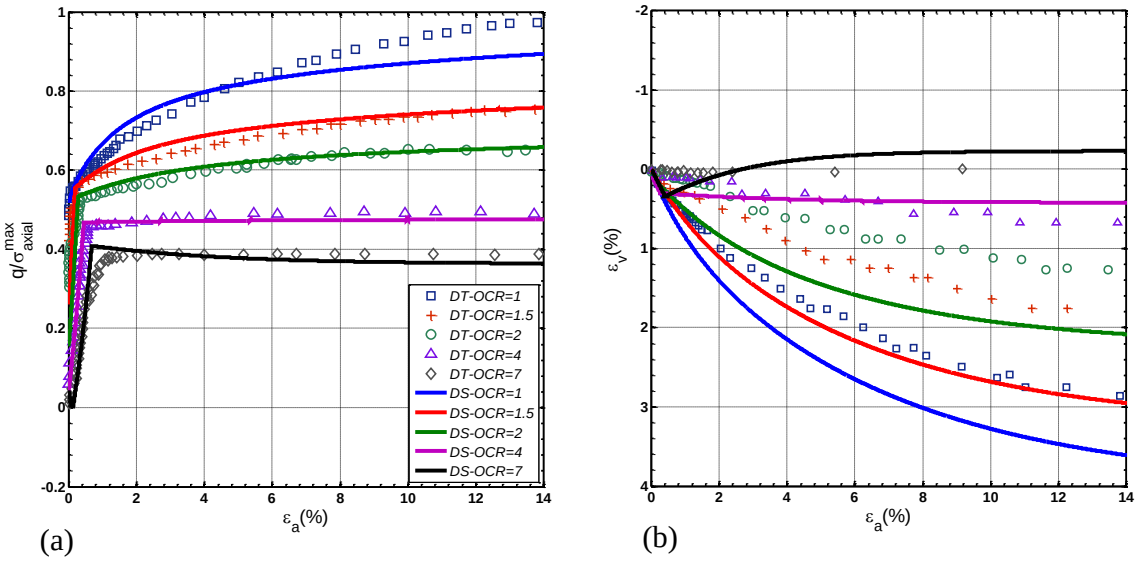

Figure 5. Comparison of SANICLAY simulations with experimental data for drained triaxial tests on K_0-consolidated samples of LCT and various OCR values (Gens [7]). **DT** an abbreviation for experimental drain tests and **DS** are for simulation of drain tests

As deduced from Figs. 2,4 and 5, the effects of consolidation history and of the induced anisotropy on the drained shearing response are significant. Notably, the differences are larger for OCR = 1, compared to OC samples. Hence, for better depicting these effects,

Fig.6 compares the data and the simulations for drained triaxial compression (CADC) tests on anisotropically consolidated samples of LCT with OCR = 1. In particular, Fig. 6 makes the comparison in the known two-plot format of Fig. 5. The various tests are differentiated in terms of the value of the consolidation stress ratio $K_c = \sigma_{r,c}/\sigma_{a,c}$, as was done in Fig. 4 for the undrained tests. It is demonstrated that the volumetric strain ε_v increases with the value of K_c, and this is thoroughly captured by the model. Furthermore, note that the $q/\sigma_{max}^{axial} - \varepsilon_{axial}$ simulations become better as the value of K_c approaches the $K_c = 0.5$, similar to undrained cases (see Fig. 4).

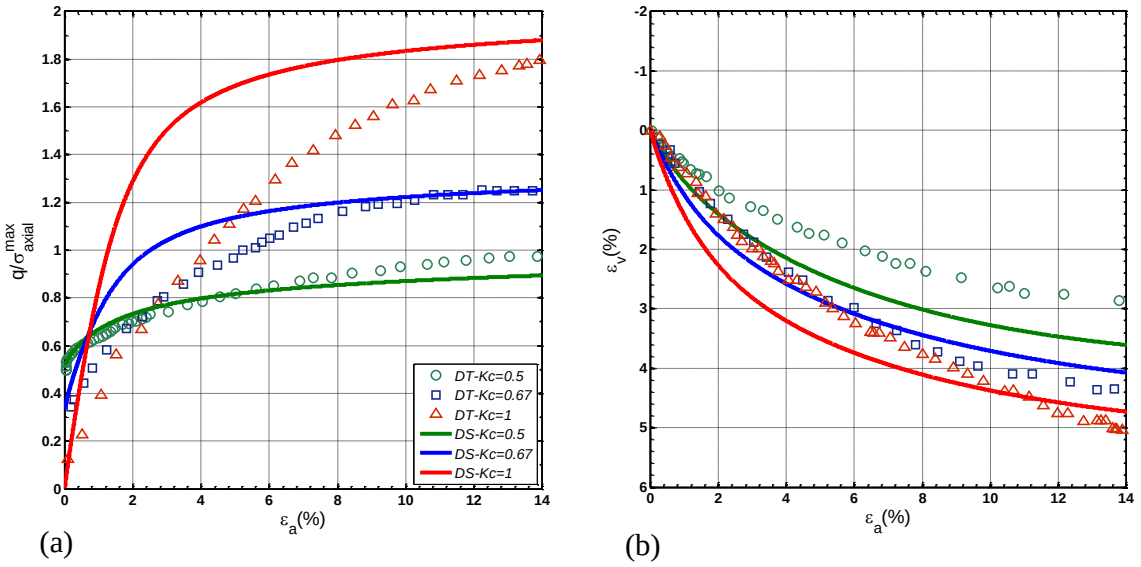

(a) (b)

Figure 6. Comparison of SANICLAY simulations with experimental data for drained triaxial tests on anisotropically consolidated samples of LCT and OCR = 1, (Gens [7])

6. CONCLUSIONS

In this paper, a semi-explicit integration scheme for the SANICLAY model has been presented and validated. Accuracy and efficiency of the proposed algorithm have been evaluated by comparing the results obtained for several drained/undrained compression/extension triaxial simulations having different OCRs with the experimental data. The results have also compared with the results obtained through the MCC model. The proposed semi-explicit algorithm does not require any iteration while integration process; however, it has an adequate accuracy and efficiency in solving the boundary value problems.

REFERENCES

1. Casagrande A, Carillo N. Shear failure of anisotropic materials, *Journal of the Boston Society of Civil Engineers*, **31**(1944) 74-87.

2. Whittle AJ. A Constitutive Model for Over consolidated Clays with Application to the Cyclic Loading of Friction Pile, Sc.D. Thesis, MIT, Cambridge, MA, 1987.
3. Ladd C, et al. Stress-deformation and strength characteristics, *Proceedings of the 9th International Conference Soil Mechanics and Foundation Engineering*, Tokyo, 1977.
4. Chen FH, Snitbhan N, Fang HY. Stability of slopes in anisotropic, non-homogenous soils, *Canadian Geotechnical Journal*, **12**(1975) 145-52.
5. Levadoux JN, Baligh MM. Pore pressure during cone penetration in clays, Report No. R. 80-15, 310, Department of Civil Engineering, MIT, 1980.
6. Sheahan TC. An Experimental Study of the Time-Dependent Undrained Shear Behavior of Re-Sedimented Clay Using Automated Stress Path Equipment, Sc.D. Thesis, MIT, Cambridge, MA, 1991.
7. Gens A. Stress-Strain and Strength of a Low Plasticity Clay, Ph.D. Thesis, Imperial College, London University, 1982.
8. Nishimura S, Minh NA, Jardine RJ. Shear strength anisotropy of natural London clay, *Geotechnique*, **57**(2007) 49-62.
9. Tavenas F, Leroueil S. Effects of stresses and time on yielding of clays, *Proceedings of the 9th International Conference of Soil Mechanics Foundations Engineering*, Tokyo, 1977.
10. Mroz Z, Norris VA, Zienkiewicz OC. An anisotropic hardening model for soils and its application to cyclic loading, *International Journal for Numerical and Analytical Methods in Geomechanics*, **2**(1978) 203-21.
11. Pietruszczak S, Mroz Z. On hardening anisotropy of K_0-consolidated clays, *International Journal for Numerical and Analytical Methods in Geomechanics*, **7**(1983) 19-38.
12. Pande GN, Sharma KG. Multilaminate model of clays-A numerical evaluation of the influence of rotation of principal stress axes, *International Journal for Numerical and Analytical Methods in Geomechanics*, **7**(1983) 397-418.
13. Schweiger HF, et al. A multi-laminate framework for modeling induced and inherent anisotropy of soils, *Geotechnique*, **59**(2009) 87-101.
14. Sekiguchi H, Ohta K. Induced anisotropy and time dependence in clays, *Proceedings of the 9th ICSMFE on Constitutive Equations for Soils* (Specialty Session 9), Tokyo, JSSMFE, 1977.
15. Hashiguchi K. An expression of anisotropy in plastic constitutive equations of soils, *Proceedings of the 9th ICSMFE, Constitutive Equations for Soils* (Specialty Session 9), Tokyo, JSSMFE, 1977.
16. Dafalias YF. An anisotropic critical state soil plasticity model, *Mechanics Research Communications*, **13**(1986) 341-7.
17. Anandarajah A, Dafalias YF. Bounding surface plasticity 3: Application to anisotropic cohesive soils, *Journal of Engineering Mechanics (ASCE)*, **112**(1986) 1292-318.
18. Whittle AJ, Kavadas MJ. Formulation of MIT-E3 constitutive model for overconsolidated clays, *Journal of Engineering Mechanics (ASCE)*, **120**(1994) 173-98.
19. Roscoe KH, Burland JB. On the generalized Stress-Strain Behavior Of 'Wet' Clay, in Engineering Plasticity, eds. Backhaus G, Cambridge University Press, Cambridge, 1968.
20. Wheeler SJ, et al. An anisotropic elastoplastic model for soft clays, *Canadian Geotechnical Journal*, **40**(2003) 403–18.

21. Dafalias YF, Manzari MT, Papadimitriou AG. SANICLAY: Simple anisotropic clay plasticity model, *International Journal for Numerical and Analytical Methods in Geomechanics*, **30**(2006) 1231-57.
22. Dafalias YF, Taiebat M. Anatomy of rotational hardening in clay plasticity, *Geotechnique*, **63**(2013) 1406-18.
23. Taiebat M, Dafalias YF, Peek R. A destructuration theory and its application to SANICLAY model, *International Journal for Numerical and Analytical Methods in Geomechanics*, **34**(2010) 1009-40.
24. Graham J, Houlsby GT. Anisotropic elasticity of a natural clay, *Geotechnique*, **33**(1983) 165-80.
25. Ortiz M, Simo JC. An analysis of a new class of integrations algorithms for elasto-plastic constitutive relations, *International Journal for Numerical and Analytical Methods in Geomechanics*, **23**(1986) 353-66.
26. Gens A, Potts DM. Critical state models in computational geomechanics, *Engineering Computations*, **5**(1987) 178-97.
27. Hashash YMA, Whittle AJ. Integration of the modified Cam-clay model in non-linear finite element analysis, *Computer Methods in Applied Mechanics and Engineering*, **14**(1992) 59-83.
28. Manzari MT, Prachathananukit R. On integration of a cyclic soil plasticity model, *International Journal for Numerical and Analytical Methods in Geomechanics*, **25**(2001) 525-49.
29. Rouainia M, Wood DM. Implicit numerical integration for a kinematic hardening soil plasticity model, *International Journal for Numerical and Analytical Methods in Geomechanics*, **25**(2001) 1305-25.
30. Simo JC, Hughes JTR. General return mapping algorithms for rate-independent plasticity, *Constitutive Laws for Engineering Materials*: *Theory and Applications*, eds. Desai CS, Krempl E, Kiousis PD, Kundu T, Elsevier Publishing Co, New York, 1987.